Two-dimensional assembly of nanoparticles grafted with charged-end-group polymers

Hyeong Jin Kim,[†] Binay P. Nayak,[†] Honghu Zhang,[‡] Benjamin M. Ocko,[¶] Alex Travesset,[§] David Vaknin,[§] Surya K. Mallapragada,[*,†] and Wenjie Wang[*,‖]

[†]Ames National Laboratory, and Department of Chemical and Biological Engineering, Iowa State University, Ames, Iowa 50011, United States

[‡]Center for Functional Nanomaterials and NSLS-II, Brookhaven National Laboratory, Upton, New York 11973, United States

[¶]NSLS-II, Brookhaven National Laboratory, Upton, New York 11973, United States

[§]Ames National Laboratory, and Department of Physics and Astronomy, Iowa State University, Ames, Iowa 50011, United States

[‖]Division of Materials Sciences and Engineering, Ames National Laboratory, U.S. DOE, Ames, Iowa 50011, United States

E-mail: suryakm@iastate.edu; wenjiew@ameslab.gov

Abstract

Hypothesis Introducing charged terminal groups to polymers that graft nanoparticles enables Coulombic control over their assembly by tuning pH and salinity of aqueous suspensions.

Experiments Gold nanoparticles (AuNPs) are grafted with poly (ethylene glycol) (PEG) terminated with CH_3 (charge neutral), COOH (negatively charged) or NH_2 group (positively charged), and characterized with dynamic light scattering, ζ-potential, and thermal gravimetric analysis. Liquid surface X-ray reflectivity (XR) and grazing incidence small-angle X-ray scattering (GISAXS) are used to determine the density profile and in-plane structure of the AuNP assembly across and on the aqueous surface.

Findings Assembly of PEG-AuNPs at the liquid/vapor interface is tunable by adjusting pH or salinity for COOH but less for NH_2 terminals. The distinct assembly behaviors are attributed to the overall charge of PEG-AuNPs as well as PEG conformation. COOH-PEG corona is the most compact and leads to smaller superlattice constants. The net charge per particle depends not only on the PEG terminal groups, but also on the cation sequestration of PEG and the intrinsic negative charge of AuNP surface. The closeness to overall charge neutrality, and the hydrogen bonding in play, brought by NH_2-PEG, enables NH_2-PEG-AuNPs assembly readily.

Graphical Abstract
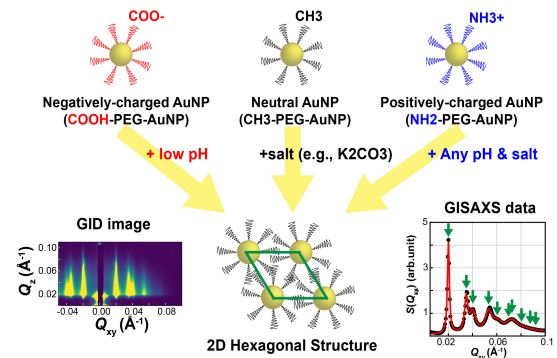
Introduction

Inorganic nanoparticles (NPs) have attracted great attention due to their unique emergent properties, which are distinct from those based on organic molecules.[1–4] For example, localized plasmon resonance, superparamagnetism, and photon upconversion can only be achieved with inorganic nanoparticles.[5–7] Self-assembly of such NPs offers a route to fabricating novel devices based on metamaterials frameworks.[8–10] A host of properties of such NP assemblies are not only dependent on the composition of the NPs, their sizes and shapes, but also on their collective responses to external stimuli, which can be tuned by their mutual arrangements and interactions.[11] Soft ligands are often used to functionalize inorganic NPs to induce interactions that can lead to assembly, where the dominant ones are the van der Waals, Coulombic, and the steric interactions.[12–14] Over the last two decades, the DNA-mediated self-assembly of colloidal superlattices has matured to the extent that a great number of complex assembly structures have been designed and built, taking advantage, by design, interparticle base-pairing hybridization.[15–18] The use of synthetic polymers as ligands, in place of DNA to mediate the interparticle interactions, is viewed as a more economic, robust and reliable approach to upscale NP-assembly. To accomplish this, water-soluble polymers, including poly(ethylene glycol) (PEG), poly(acrylic acid) (PAA), and poly(N-isopropylacrylamide) (PNIPAM) have been used as NP surface ligands to mediate both two- and three-dimensional superlattice formation of gold nanoparticles (AuNPs) at the liquid/vapor interface and in aqueous bulk solutions under variable mild solvent conditions (e.g., pH, salinity, and temperature).[19–31] Nevertheless, most NP superlattices are built with charge-neutral ligand functionalized NPs, where the assembly process is mainly driven by the balance between van der Waals attractive forces and steric conformations among polymeric ligands. In crude analogy, using single stranded DNA to functionalize metal NPs, where the terminal groups are complementary base-paired, has been shown to produce a plethora of binary superstructures.[18] To introduce similar complimentary interaction, we graft AuNPs with polymeric ligands that have charged terminals to create "super-ions", and expect their assembly behaviors vary in response to changing suspensions conditions (pH or salinity). Our long term goal is to discover binary systems where Coulombic interactions among such super-ions can be tuned to form colloidal clusters, assemblies, and superstructures analogous to ionic crystals.[32–36]

In this study, we explore the assembly of AuNPs that are functionalized with thiolated PEG terminated with either carboxylic (COOH) or amine (NH_2) groups. These end-groups render net surface charge to the functionalized NPs and we exploit them as another means to control PEG-AuNP assembly and crystallization. In the past, other controls such as pH, salinity, temperature, and poly-electrolyte co-solutes have been used to effectively mediate ordered assembly of charge neutral PEG-AuNPs.[19–25,27–30] Here, we compare the self-assembly on the aqueous surface of suspensions of like-charged PEG-AuNPs with a positive, negative, or neutral charge. We note that the mechanisms of colloidal assembly of like-charged colloidal particles, based on the Deryaguin–Landau–Verwey–Overbeek theory (DLVO), have been investigated extensively and are still debated.[37–41]

In the present study, PEG-AuNPs accumulate on the aqueous surface and form a two-dimensional (2D) assembly.[19] We utilize synchrotron-based liquid surface X-ray diffraction methods, including X-ray reflectivity (XR) and grazing-incidence small angle X-ray scattering (GISAXS), to determine the 2D films at the vapor/liquid interface. This study adds to previous assembly studies using neutral PEG as a surface modifier of the AuNPs.

Experimental Section

Preparation of Materials

Citrate-stabilized gold nanoparticles (AuNPs) of ~ 10 nm diameter were purchased from Ted

Pella. Thiolated poly(ethylene glycol) (HS-PEG; molecular weight of $\sim$ 5 kDa) terminated with carboxyl (COOH-), methyl (CH$_3$-), or amine (NH$_2$-) group were obtained from Creative PEGWorks. AuNPs were functionalized with HS-PEG-COOH, HS-PEG-CH$_3$, or HS-PEG-NH$_2$ by ligand-exchange protocol.[30] Briefly, thiolated PEG was dissolved in aqueous solution of sodium chloride (NaCl; 1M). Then, it was incubated with AuNP suspensions for 2 to 3 days. PEG grafted AuNPs (PEG-AuNPs) were purified by centrifugation three times. In this study, we use PEG-AuNP to denote PEG grafted AuNPs in general, and x-PEG-AuNP to specify the PEG ligands of AuNPs terminated with x group (i.e., CH$_3$, COOH, or NH$_2$ groups). For example, COOH-PEG-AuNPs refers to gold nanoparticles functionalized with carboxyl-terminated PEG. The PEG-AuNP concentrations were determined by Ultraviolet–visible (UV–vis) absorption spectroscopy measurements (calibrated and standardized with vendor provided information, Molecular Devices, SpectraMax M3) and adjusted to be at approximately 20 nM. Further dynamic light scattering (DLS) characterization of the grafted AuNPs was conducted with a NanoZS90 and its associated software Zetasizer (Malvern, U.K.). The DLS intensity percentage versus particle hydrodynamic size distribution profiles clearly show an increase in size upon grafting with all three PEGs. (see Table 1 and Figure 1). Compared to CH$_3$-PEG-AuNPs, the hydrodynamic size of COOH-PEG-AuNPs is 18% smaller while that of NH$_2$-PEG-AuNPs is 5% larger. Zeta (ζ) potential measurements, also conducted with NanoZS90, were used to quantify the surface charge of PEG-AuNPs as listed in Table 1. The electrical polarity of COOH-PEG-AuNPs and NH2-PEG-AuNPs, along with enlarged hydrodynamic size, ensures successful grafting of PEG with distinct terminal groups.

To determine the average grafting density of PEG on each particle surface, thermogravimetric analysis (TGA) of PEG-AuNPs was conducted with Netzsch STA449 and its associated software Proteus. The grafted NPs are degraded in a temperature range between 100

to 600 °C under argon gas. PEG on AuNP surfaces was found to be thermally degraded between 350 to 450 °C (shown in Fig. S1).[30] The grafting density for each sample was calculated using Eq. S1 and is summarized in table 1.[42]

K$_2$CO$_3$ stock solutions were prepared at a sufficiently high concentrations that could be added in small amounts to the grafted nanoparticle suspensions at specified concentrations for the X-ray scattering experiments (see Supporting Information for pH determination). The HCl, NaOH, and K$_2$CO$_3$ solutions are treated as ideal solutions and their ionic strength is calculated as $\frac{1}{2}\sum_i c_i Z_i^2$, where c_i and Z_i are the concentration and valance of ions of species i.
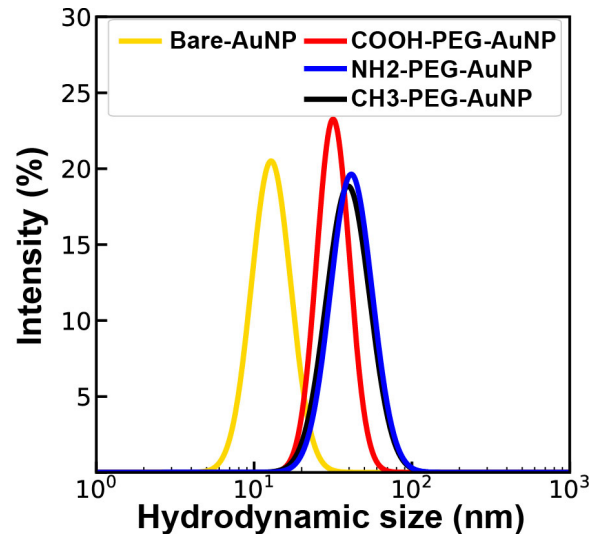
Figure 1: DLS intensity percentage versus hydrodynamic size distribution for the suspensions of bare surface and polymer grafted AuNPs in the absence of salts.

X-ray Experimental Setup

In-situ liquid surface X-ray scattering experiments were carried out at the SMI beamline open platform liquid surfaces (OPLS) end station at the National Synchrotron Light Source II (NSLS-II), Brookhaven National Laboratory, with incident X-ray energy 9.7 keV. X-ray reflectivity (XR) and grazing-incidence small angle X-ray scattering (GISAXS) were used to investigate the 2D assembled films at the liquid/vapor interface using area detectors. Data correction and reduction were conducted onsite with the beamline routines. Experimental setups and more details can be found else-

Table 1: DLS, ζ potential and Grafting density values

	DLS		TGA		
End group of grafted PEG	Hydrodynamic size (nm)[1]	ζ potential (mV)	Initial weight (mg)	Changed weight[3]	Grafting density (chains/nm^2)
n.a.[2]	12.7(1)	-38.5 ± 2.3	-	-	-
-CH$_3$	39.1(2)	-14.5 ± 1.8	1.98	30%	1.6 ± 0.05
-COOH	31.8(3)	-29.4 ± 2.1	2.05	30%	1.5 ± 0.10
-NH$_2$	41.0(4)	$+13.6 \pm 2.6$	1.58	32%	1.7 ± 0.15

[1] Only the modal size on the distribution profile is reported.

[2] The bare surface AuNPs, stabilized with citrate ligands.

[3] The changed weight was calculated from Fig. S1 and is relative change with respect to initial weight.

where.[19,30] Below is a brief description of the methodology. The X-ray reflectivity (XR), R, is measured as a function of Q_z that is the vertical component of the scattering vector, $\vec{Q}$, and is normalized to the calculated Fresnel reflectivity, R_F, for the aqueous solutions. Calculated R/R_F profiles to fit the data are obtained and refined with a parameterized multi-slab model that generates the electron density (ED) profile along the surface normal (i.e., depth in z-direction), $\rho(z)$, via Parratt's method that best fits the data.[43]

The grazing incidence small-angle scattering (GISAXS) intensity data is recorded as a two-dimensional function of Q_{xy} and Q_z, where Q_{xy} is the horizontal component of $\vec{Q}$. A linecut intensity profile of GISAXS, as a function of Q_{xy} is integrated over Q_z range 0.01–0.03 Å^{-1}, denoted as $I(Q_{xy})$. The Bragg-reflection peaks on $I(Q_{xy})$ profiles are associated with a real-space, two-dimensional lattice. The linecut profile $I(Q_{xy})$ divided by the calculated form factor intensity profile by a single nanoparticle,[19,21,30] is denoted as $S(Q_{xy})$, which is proportional to the structure factor that describes the spatial correlation among particles.[43]

Results and Discussion

In this section, we compare the surface X-ray scattering results to determine the impact of the charge of the PEG terminal group on aqueous surface NP assembly at room temperature.

By tuning the salinity or pH of the aqueous suspensions and based on previous results, we expect the PEG-AuNPs to populate the aqueous surface and assemble into ordered lattices. The XR measurements from the aqueous suspensions provide the electron densities of the enriched surfaces, while the GISAXS measurements provide in-plane NPs arrangement information.[19]

1. Salt induces 2D assembly.

K$_2$CO$_3$ is among the most effective salts to induce ordered assembly of AuNPs grafted with neutral PEG ligands, CH$_3$-PEG, in aqueous suspensions.[19] This is generally attributed to the salting-out of PEG in response to a poorer solvent enriched with salts.[19,21,22] Figure 2 shows normalized reflectivities, R/R_F, for PEG-AuNPs in aqueous solutions at various K$_2$CO$_3$ concentrations. In pure aqueous suspensions without salt, i.e., [K$_2$CO$_3$]=0 mM (Fig. 2(a)), the R/R_F profiles of CH$_3$-PEG-AuNPs and COOH-PEG-AuNPs suspensions fall off monotonously with Q_z, similar to that of a bare and smooth liquid/vapor interface. The lack of Q_z-dependent modulation does not support surface NP adsorption. Meanwhile, the R/R_F profile for NH$_2$-PEG-AuNPs shows a prominent interference pattern. This is evidence for the spontaneous formation of a thin film of NH$_2$-PEG-AuNPs at the vapor/liquid interface. This is surprising since the amine group presumably renders a positive charge at the sur-
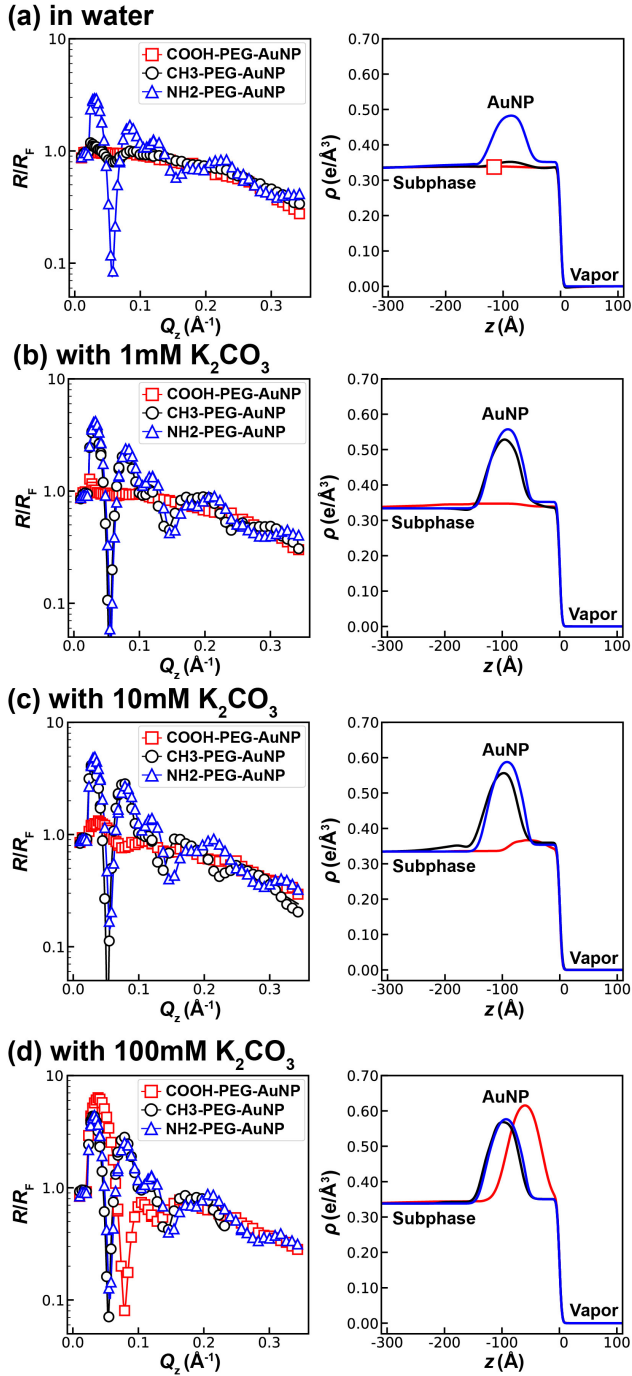
Figure 2: Left: R/R_F data COOH-, CH$_3$-, NH$_2$-PEG-AuNPs under various solvent conditions as indicated. Right: Their corresponding electron density (ED) profiles are provided.

face of the PEG-corona for each AuNP. It is therefore expected that such charged AuNPs would tend to be fully dispersed (soluble) in aqueous suspensions due to Coulombic interparticle repulsion. However, these repulsive interactions can be weakened by charge screening of co-ions and the salting-out of PEG. With the addition of 1 mM K$_2$CO$_3$, in Fig. 2(b), the R/R_F of CH$_3$-PEG-AuNPs is very similar

to that of NH$_2$-PEG-AuNPs, where the latter remains practically unchanged upon addition of K$_2$CO$_3$, i.e, formed film is almost saturated even at 0 mM K$_2$CO$_3$. The negatively-charged COOH-PEG-AuNPs exhibits a distinctive interference pattern in R/R_F at 10 mM K$_2$CO$_3$, with a much stronger effect at 100 mM K$_2$CO$_3$, as shown in Fig.2 (c) and (d).

The corresponding ED profiles across the interfaces obtained by fitting the R/R_F are shown in the right panel of Fig. 2. The bell-shaped peak with high ED represents a uniform layer formed by the electron-rich AuNPs, and the ED excess on both sides of the AuNPs film is attributed to PEG. We note that it is difficult to distinguish the PEG protruding into the aqueous suspension as its ED is close to that of water.[22] A summary of inspections of ED profiles is as follows: 1. The threshold of bulk [K$_2$CO$_3$], above which the surface enrichment of PEG-AuNPs are observed, is ranked as: NH$_2$-PEG-AuNPs $<$ CH$_3$-PEG-AuNPs $<$ COOH-PEG-AuNPs. The NH$_2$-PEG-AuNPs spontaneously populate and saturate the aqueous surface without any salt as their surface density is practically insensitive to the further addition of K$_2$CO$_3$. The CH$_3$-PEG-AuNPs populate the surface sporadically at [K$_2$CO$_3$]=0 mM and vastly after the addition of 1mM K$_2$CO$_3$. The COOH-PEG-AuNPs require a larger amount of K$_2$CO$_3$ (10-100 mM) to fully populate the surface. 2. Once the surfaces are saturated, the ED profiles for CH$_3$-PEG-AuNPs and NH$_2$-PEG-AuNPs are almost indistinguishable, and both feature a flat ED transition zone between vapor phase ($\rho = 0$) and the bell-shaped high-ED zone that is mostly of Au cores.[31] This flat ED zone is attributed to the compressed PEG ligands that are in the immediate vicinity of the vapor phase.[29] In contrast, the lack of such compressed PEG sub-layer for COOH-PEG-AuNPs films is reminiscent of previously studied PNIPAM-AuNPs films where the PNIPAM ligands collapse on the AuNP surface upon salt addition and assembly.[26] The scenario that the PEG chains partially collapse is manifested by the DLS results where the modal hydrodynamic size and size distribution are smaller and narrower for COOH-PEG-AuNPs than the other
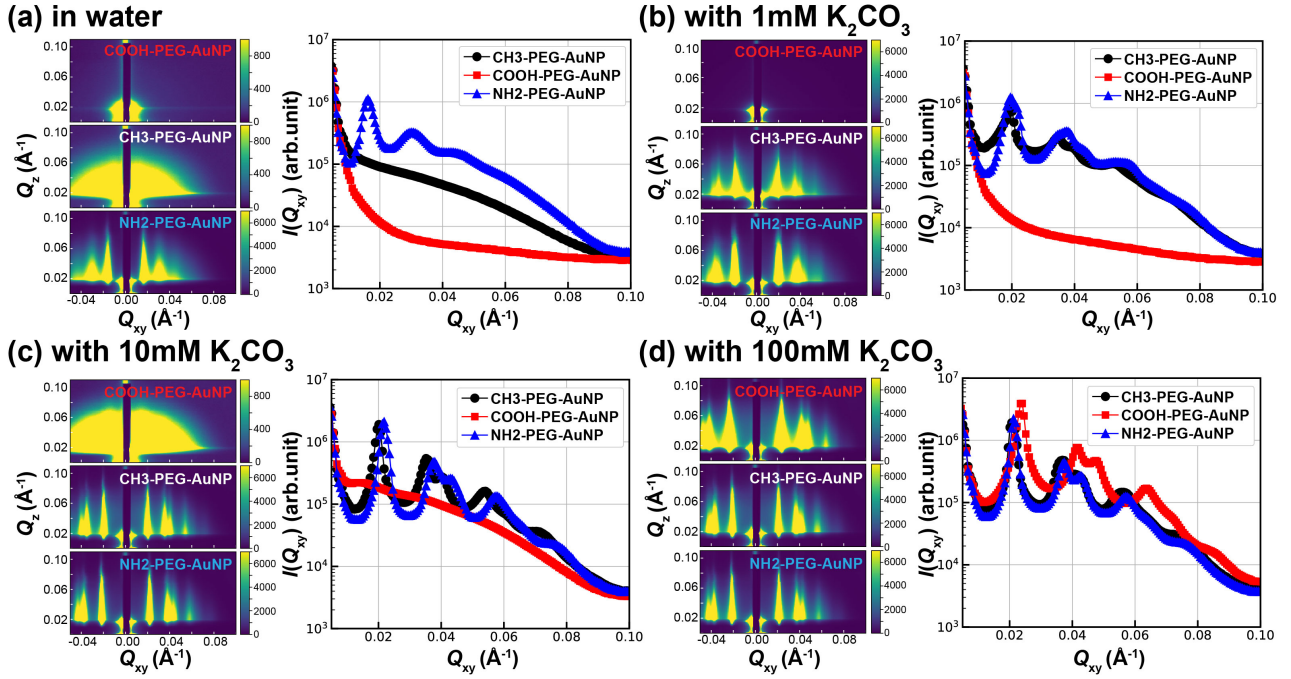
Figure 3: (a-d) Left: GISAXS patterns for COOH-, CH$_3$-, NH$_2$-PEG-AuNPs under various solvent conditions as indicated. Right: Their horizontal linecut intensity profiles integrated over Q_z range $0.01 - 0.03$ Å^{-1} are plotted on a logarithmic scale.

counterpart terminal groups.
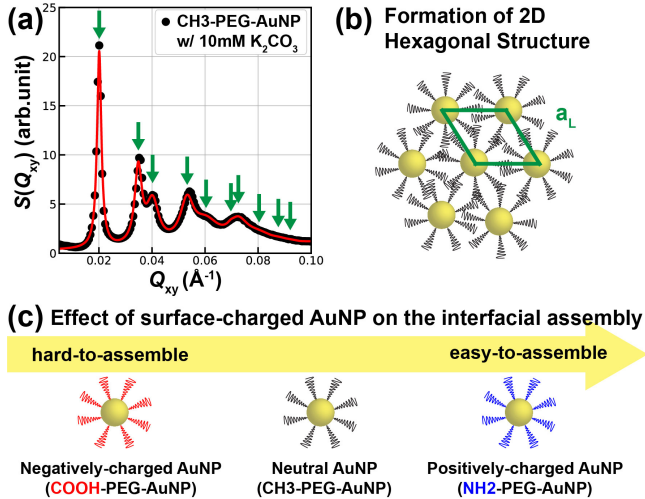
Figure 4: (a) $S(Q_{xy})$ profile proportional to the in-plane structure factor for methyl-terminated PEG-AuNPs at 10 mM K$_2$CO$_3$ (black circles). Red solid curve is the best-fit using a 2D hexagonal lattice. Green arrows indicate the Q_{xy} positions of Bragg diffraction peaks for 2D hexagonal lattice. (b) Illustration for 2D hexagonal lattice of PEG-AuNPs with a lattice constant, a_L. (c) Schematic representation of effects of surface-charged AuNPs on the interfacial assembly.

To complement the main findings from the XR above, we present and analyze in-plane diffraction results from the same films using GISAXS. The GISAXS results are presented using two-dimensional colormaps of the scattering-intensity as a function of Q_z and Q_{xy},

shown in Figure 3. In general, for a bare vapor/liquid interface, the GISAXS map is dominated by the diffuse scattering tail of the reflected X-ray primary beam and the beam-stop. Typical scattering images are shown in Figure 3. The upper left panel of Fig.3(a) shows the image for COOH-PEG-AuNPs without any salt added, indicating a bare surface. The absence of additional features, except from the direct beam, is consistent with the conclusion from the XR results that the COOH-PEG-AuNPs in the absence of salts do not populate the surface. For CH$_3$-PEG-AuNPs without salt the GISAXS map shows a broad isotropic halo arising from the form-factor of AuNPs that sparsely populate the surface and lack spatial correlations. XR is mostly insensitive to such details, but is indirectly manifested by a very weak peak in R/R_F at low Q_z values that deviates from that of an ideal bare liquid surface (see Fig. 2(a)). For NH$_2$-PEG-AuNPs in the absence of salts, the GISAXS pattern shows a few broad rod-like Bragg-reflections (e.g., Figure 3(a) bottom left panel), modulated by the AuNP form-factor mentioned above. Such rod-like features result from spatially ordered AuNPs confined in 2D films at the liquid/vapor interface.

At [K$_2$CO$_3$]= 1 mM, COOH-PEG-AuNPs are

6
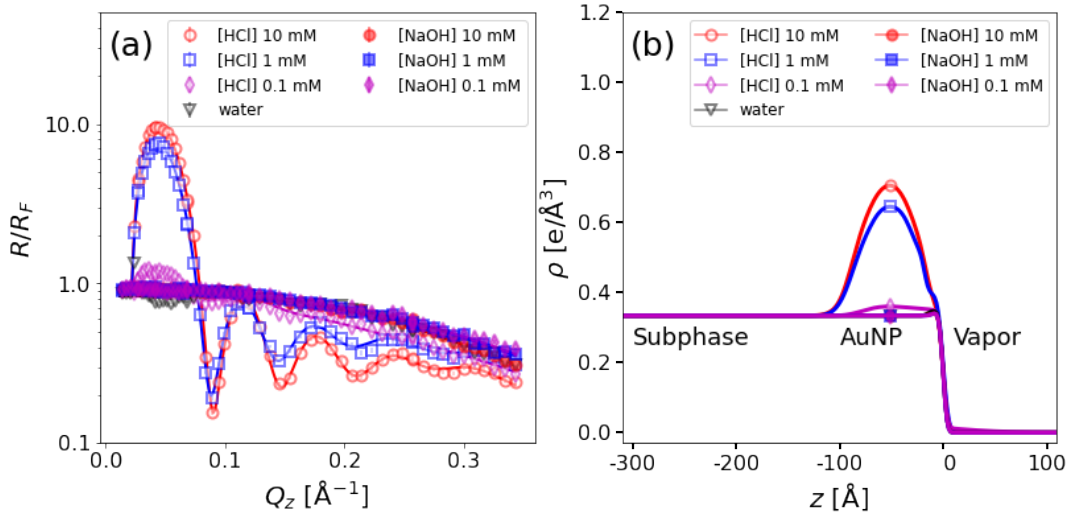
Figure 5: (a) R/R_F data on logarithmic scale for carboxyl-terminated (COOH-) PEG-AuNPs under various solvent conditions as indicated. (b) Corresponding electron density (ED) profiles that best fit R/R_F data in (a).

still dispersed in the bulk of the suspension and do not migrate to the liquid/vapor interface. However, both NH$_2$- and CH$_3$-PEG-AuNPs at this same salt concentration show similar but sharper Bragg-reflection rods, consistent with our XR results that show a uniform film formation. At [K$_2$CO$_3$]= 10 mM, COOH-PEG-AuNPs show the form-factor-like pattern of AuNPs that indicates partial population at the surface, with no correlations among particles (Fig. 3(c)). This is consistent with the XR data showing excess ED at the surface (Fig. 2(c)). At this concentration, the NH$_2$- and CH$_3$-PEG-AuNP show much sharper and additional Bragg-reflections. At [K$_2$CO$_3$]= 100 mM, the images for COOH-PEG-AuNPs show a strong diffraction pattern, similar, but shifted to larger Q_{xy} values compared, to the patterns of NH$_2$- and CH$_3$-PEG-AuNPs systems. The shift of diffraction pattern to larger Q_{xy} suggests shorter inter-particle separations for COOH-PEG-AuNPs, in accordance with the thinner or collapsed PEG corona supported by DLS and XR, respectively.

To quantify the observed patterns, we display, side-by-side, line-cuts form the 2D maps obtained by integrating the intensity over a finite Q_z range ($0.01 - 0.03$ Å^{-1}). The line-cuts clearly show AuNP form-factor for CH$_3$-PEG-AuNPs at [K$_2$CO$_3$]=0 mM and for COOH-PEG-AuNPs at [K$_2$CO$_3$]=10 mM. At these concentrations, the in-plane Bragg reflections of

NH$_2$-PEG-AuNPs are quite broad, indicating in-plane hexagonal short-range order. As the concentration increases further all three systems show sharper diffraction peaks that can be indexed by a two-dimensional hexagonal lattice where up to 7th order reflection is observed. For demonstration, Fig. 4(a) shows the in-plane diffraction pattern, $S(Q_{xy})$, from the 2D hexagonal structure of CH$_3$-PEG-AuNPs (at 10 mM K$_2$CO$_3$) with arrows marking the calculated Bragg reflection positions for this structure shown in Fig. 4 (b). Similar structures are also formed by NH$_2$-PEG-AuNPs and COOH-PEG-AuNPs. Combining GISAXS, XR and DLS results, we conclude that the COOH terminal group induces some kind of partial polymer collapse, such that the effective radius of the COOH-PEG-AuNPs is smaller than the ones grafted with the other terminal groups. The extracted structural parameters for the XR and the GISAXS are listed in Table 2.

2. pH tunes the threshold for assembly of COOH-PEG-AuNPs.

The effect of pH on the assembly of CH$_3$-PEG-AuNPs has been previously investigated.[22,44] These studies show that tuning pH with equal [HCl] or [NaOH] has same effect on assembly of CH$_3$-PEG-AuNPs.[44]

It is expected that lowering the pH of the suspension will result in protonation of the car-

(a) COOH-PEG-AuNP with HCl

(b) COOH-PEG-AuNP with NaOH

(c)

Negatively-charged

COO-

COOH-PEG-AuNP
in water

Decreasing pH
(add HCl)

Increasing pH
(add NaOH)
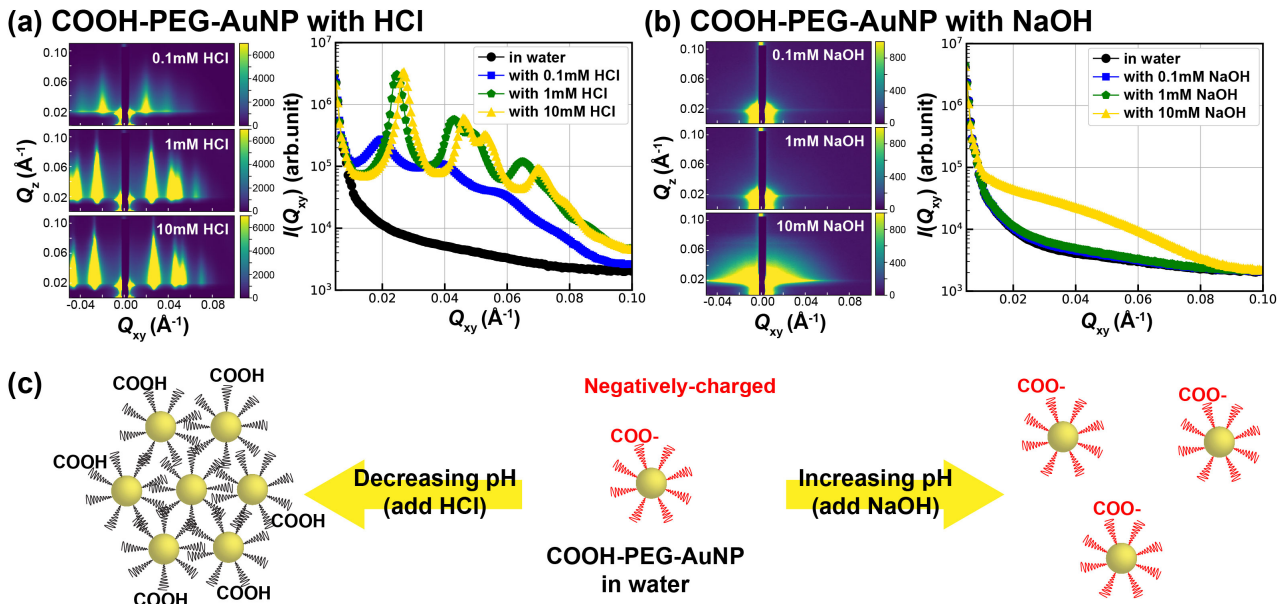
Figure 6: (a-b) Left: GISAXS patterns for carboxyl-terminated PEG-AuNPs under various solvent conditions as indicated. Right: Their horizontal linecut intensity profiles are plotted on a logarithmic scale. (c) Schematic representation of assembling behavior of carboxyl-terminated PEG-AuNPs (negatively-charged) by pH changes.

boxylic terminals, neutralizing the PEG corona shells, and inducing 2D aggregation of charge neutral COOH-PEG-AuNPs at the liquid/ vapor interface. In contrast, adding NaOH is expected to promote deprotonation and more negatively charge the $COOH/COO^-$-PEG-AuNPs surface hence favoring solubility. Figure 5 shows R/R_F profiles for COOH-PEG-AuNPs at different pH levels via the addition of HCl or NaOH. It shows that adding HCl promotes 2D assembly while adding NaOH does not, as expected. We also note that by adding salt or lowering the pH the R/R_F for COOH-PEG-AuNPs displays distinct features. Lowering the pH has a higher first maximum and higher minimum, compared to other two terminal groups with K_2CO_3 shown above. These kind of R/R_F profiles are similar to those observed for AuNPs that are grafted with Poly(N-isopropylacrylamide) (PNIPAM) for which the conclusion drawn was that the polymer chains partially collapse toward the surface of the core AuNPs,[26,45] thus allowing for higher surface population of AuNPs. On the other hand, R/R_F profiles do not exhibit interference ripples for [NaOH] > 0.1 mM, suggesting only marginal surface population of COOH-PEG-AuNPs.

GISAXS results shown in Figure 6 are consistent with the XR results shown in Fig. 5.
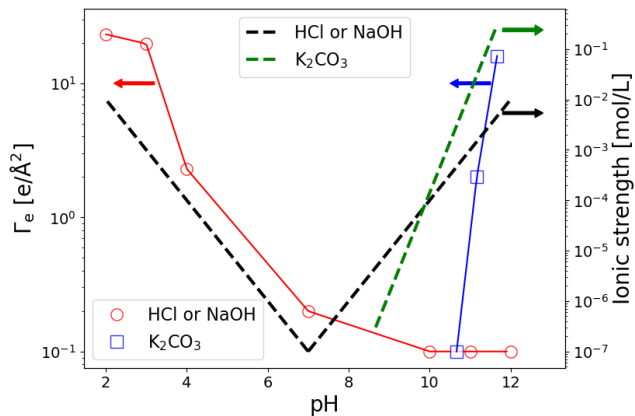
Figure 7: The surface electron excess, Γ_e, as a function of pH tuned by HCl, NaOH, or K_2CO_3 for COOH-PEG-AuNP suspensions. Dashed lines are calculated ionic strength for HCl, NaOH and K_2CO_3 solutions as a function of pH.

At neutral pH where the suspension has no salt K_2CO_3, HCl, or NaOH, the GISAXS patterns and line-scans mainly originate from the background, manifested as featureless, falling-off line-cut intensity curves. Upon lowering the pH (i.e., increasing [HCl]), Bragg rods emerge at pH 4.0 and become sharper at pH 3.0 and below. The Bragg rods are at positions expected for a 2D hexagonal lattice of AuNPs at the vapor/ liquid interface. In contrast, at higher pH (i.e., increasing [NaOH]), the GISAXS results resemble that found at neutral pH, suggesting absence of surface enrichment. However, at the
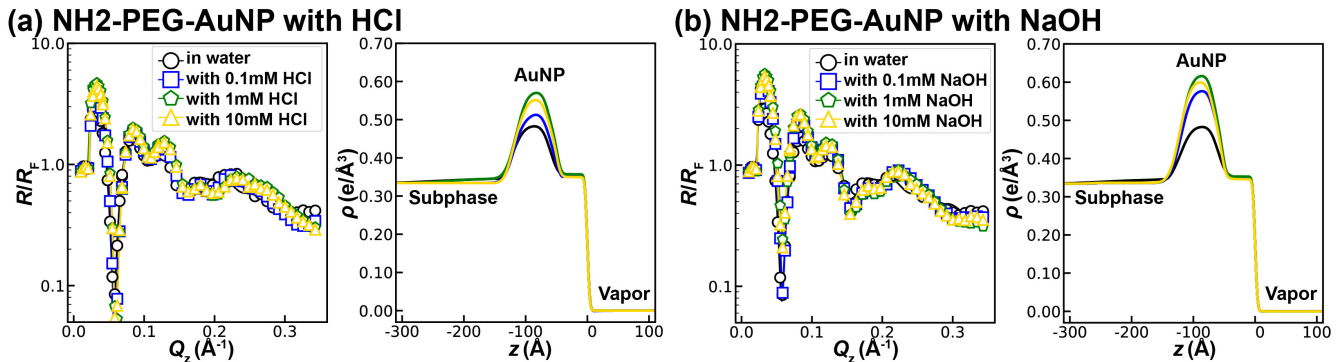
Figure 8: (a,b) Left: R/R_F data for amine-terminated PEG-AuNPs under various solvent conditions as indicated. Right: Their corresponding electron density (ED) profiles are provided.

highest pH tested, pH 12.0 (i.e., [NaOH]=10 mM), the line-cut intensity profile resembles that of the AuNP form factor, indicating the surface bound AuNPs have accumulated at the air/water interface, albeit without long-range in-plane order. We speculate that larger pH values may lead to long-range in-plane order.We note that at very large NaOH concentrations, the co-ion, i.e., Na^+, may bind back to the COO^- group making the PEG-AuNP surface more close to charge neutral and hence induce particles' migration to the surface. Such a phenomena is similar to the one observed, but for the oppositely charged amine headgroup monolayer, that at very low pH the co-ion (Cl^- in this case) starts neutralizing the head group.[46] In the Theoretical Considerations section, we explore more probable cause in terms of PEG and ion interactions.

Both XR and GISAXS results suggest that the COOH-PEG-AuNPs can be treated as super-ions where their electrostatic interaction strength can be manipulated with pH, as shown in Figure 6(c). The charged state of the super-ions depends on deprotonation and protonation on their PEG corona. At sufficiently high [HCl], the carboxylic terminals are fully protonated and become near charge neutral, and particles assemble in the presence of ions. Abundance of Cl^- attributes to poor solvent for PEG, and assembly states are favored as the van der Waals interaction among PEG ligands kicks in. But for pH > 7, the carboxylic terminals are deprotonated and thus charged, leading to repulsive interactions among like-charge super-ions. The repulsive interaction trumps the attractive

interaction among PEG ligands and counteracts aggregation. However, the attractive interactions may trump repulsive interaction once ionic contents increase (i.e., Na^+ and OH^-), as shown in Figure 6(b). Indeed, the results with K_2CO_3 at similar pH level as NaOH but significantly higher ionic strength also show that COOH-PEG-AuNPs assemble at $[K_2CO_3]=100$ mM, which has orders of magnitude higher ionic strength than 10 mM NaOH (similar pH level). Our comment above about the possibility of of co-ion (e.g., Na^+) binding at large pH values (i.e., high NaOH concentration) can also be found in Ref. [46].

In summary, the charged COOH-terminals seemingly dictate repulsive and attractive interactions that are tunable by pH and salinity, respectively. Figure 7 summarizes the surface electron excess, Γ_e, a measure of surface enrichment of AuNPs, as a function of pH tuned by HCl, NaOH, or K_2CO_3 individually.

3. pH affects NH$_2$-PEG-AuNPs similar to CH$_3$-PEG-AuNPs.

NH$_2$-PEG-AuNPs suspensions can also be expected to respond to pH manipulation, through the addition of HCl or NaOH. Surprisingly, for NH$_2$-PEG-AuNPs lowering or increasing pH levels leads to an increase of the peak in the AuNP ED, as shown in Fig. 8 (a) and (b). At neutral pH there is spontaneous monolayer formation at the liquid/vapor interface for NH$_2$-PEG-AuNPs. There is prominent surface ED enrichment of NPs regardless of pH levels. This is similar to earlier results for CH$_3$-
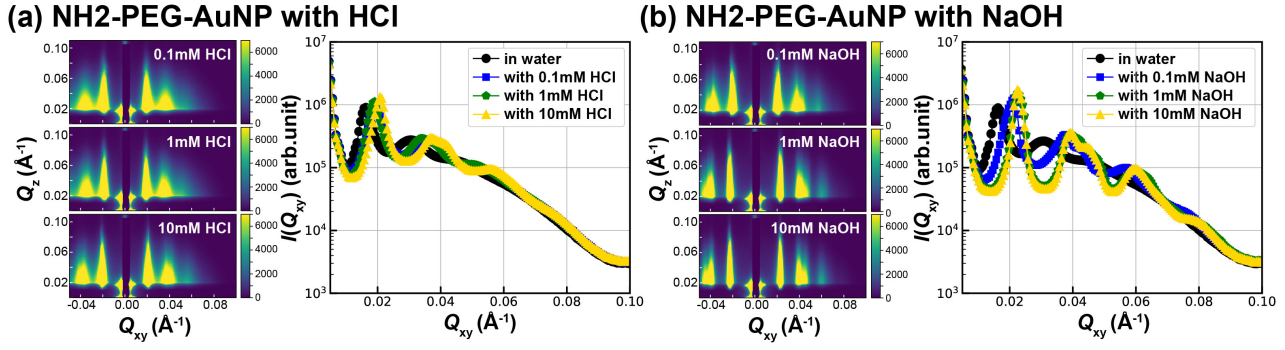
Figure 9: (a-b) Left: GISAXS patterns for amine-terminated PEG-AuNPs under various solvent conditions as indicated. Right: Their horizontal linecut intensity profiles are plotted on a logarithmic scale.

Table 2: GISAXS and XR results for carboxyl-terminated (COOH-), methyl-terminated (CH3-), and amine-terminated (NH2-) PEG-AuNPs under various solvent conditions as indicated.

End group of grafted PEG	Solvent condition	GISAXS results	a^*(nm)	Γ_e^{**} (e/Å^2)
-CH$_3$	pure water	Form factor	n.a.	< 0.5
-CH$_3$	1mM K$_2$CO$_3$	2D hexagonal structure	~ 37	~ 12
-CH$_3$	10mM K$_2$CO$_3$	2D hexagonal structure	~ 36	~ 17
-CH$_3$	100mM K$_2$CO$_3$	2D hexagonal structure	~ 34	~ 16
-COOH	pure water	Background-like	n.a.	< 0.5
-COOH	1mM K$_2$CO$_3$	Background-like	n.a.	< 0.5
-COOH	10mM K$_2$CO$_3$	Form factor	n.a.	~ 2
-COOH	100mM K$_2$CO$_3$	2D hexagonal structure	~ 32	~ 16
-NH$_2$	pure water	2D hexagonal structure	~ 44	~ 11
-NH$_2$	1mM K$_2$CO$_3$	2D hexagonal structure	~ 36	~ 14
-NH$_2$	10mM K$_2$CO$_3$	2D hexagonal structure	~ 33	~ 17
-NH$_2$	100mM K$_2$CO$_3$	2D hexagonal structure	~ 33	~ 16
-COOH	0.1mM HCl	2D hexagonal structure	~ 38	~ 2
-COOH	1mM HCl	2D hexagonal structure	~ 29	~ 20
-COOH	10mM HCl	2D hexagonal structure	~ 27	~ 23
-COOH	0.1mM NaOH	Background-like	n.a.	< 0.5
-COOH	1mM NaOH	Background-like	n.a.	<0.5
-COOH	10mM NaOH	Form factor	n.a.	< 0.5
-NH$_2$	0.1mM HCl	2D hexagonal structure	~ 38	~ 12
-NH$_2$	1mM HCl	2D hexagonal structure	~ 38	~ 17
-NH$_2$	10mM HCl	2D hexagonal structure	~ 35	~ 14
-NH$_2$	0.1mM NaOH	2D hexagonal structure	~ 34	~ 16
-NH$_2$	1mM NaOH	2D hexagonal structure	~ 32	~ 19
-NH$_2$	10mM NaOH	2D hexagonal structure	~ 32	~ 17

* For 2D hexagonal structure, lattice constant, $a = 4\pi/(\sqrt{3}Q_1)$. ** The excess of surface electron density in ED profiles, $\Gamma_e = \int[\rho(z) - \rho_{\mathrm{sub}}(z)]\mathrm{d}z$.

PEG-AuNPs, which show that what is needed to induce assembly are ions (electrolytes) in the suspension.[20] Fig. 9 shows GISAXS intensity colormaps and and line-cuts for low pH (with HCl) and at high pH (with NaOH). The line-cut profiles show that the diffraction pattern shifts to larger Q_{xy} values with either incremental or decremental pH from neutral. This indicates a decreasing lattice constant of the hexagonal lattice. Such a decrease in lattice

constant is consistent with the increase in surface density determined from XR analysis (See Table 2). Although lowering the pH increases the AuNPs density at the surface, the GISAXS peaks are broader than those for an ideal hexagonal crystal (see Fig. 4 where adjacent hexagonal peaks can be resolved). On the other hand, the increase in pH yields higher-quality crystals with better-resolved peaks, indicating the assembly behavior is influenced by amine terminals. Structural parameters extracted from the XR and GISAXS for NH_2-PEG-AuNPs are listed in Table 2.

Theoretical Considerations

Below, we initiate some theoretical considerations to shed light on the seemingly distinct assembly behaviors of COOH-PEG-AuNPs and NH_2-PEG-AuNPs in response to varying pH and ionic strength. We use the Poisson-Boltzman (PB) theory to calculate the actual charge for each PEG-AuNP in accordance to measured ζ potentials and discuss other competing interactions that are not included in the PB theory.

We assume a gold nanoparticle of core diameter D_{NP} functionalized with PEG with either terminal amine or carboxylic groups. As shown in Table 1, the bare, unfunctionalized AuNP is negatively charged. This is expected, since as reported in Ref. [47], it is not entirely possible to make the AuNP electrically neutral. Within PB, the ζ potential, normalized by the Boltzmann constant k_B and temperature T, is given by:

$$\frac{e\zeta}{k_B T} = 2 \frac{\text{sign}(\sigma)}{\hat{\lambda}_{GC}} \frac{\hat{R}}{1 + \hat{R}} \qquad (1)$$

where $\hat{R} = R_h/\lambda_{DB}$, $\hat{\lambda}_{GC} = \lambda_{GC}/\lambda_{DB}$ with R_h the nanoparticle (hydrodynamic) radius and λ_{GC}, λ_{DB} the Guoy-Chapman and Debye lengths, respectively and σ the overall charge density (see Supporting Information for further details). The sign function returns 1, 0, and -1 if the argument σ is positive, zero, or negative, respectively.

Using the measured values for the nanoparticle hydrodynamic radius (or diameter) and the ζ potential, we calculate the net charge (from the Guoy-Chapman length) per NP for each case. We then use this information to draw some qualitative considerations. The charge state of the PEG-AuNPs are conceptually shown in Fig.10. The total net charge per AuNP obtained based on Table 1 gives respectively:$-45e$ per bare AuNP, $-17e$ per CH_3-PEG-AuNP, $-27e$ per COOH-PEG-AuNP, and $+16e$ per NH_2-PEG-AuNP, where e denotes the elementary charge.
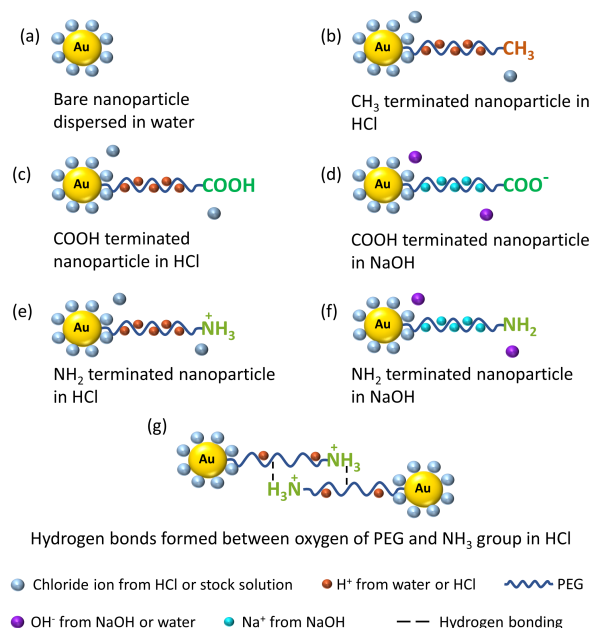
Figure 10: (a) Bare surface AuNPs carry net negative charges due to residual Cl^- ions. (b) PEG binds protons, hydroniums and cations, thus appears positively charged and offsets the negative charge of the core AuNP surface. (c) Both PEG and COOH bind proton and appear positively charged in a H^+ abundant environment. However, the carboxyl group is protonated and remain charge neutral. (d) In a high pH environment, PEG binds Na^+ and appears positively charged, but the carboxyl group is deprotonated and carry negative charge, which diminishes the reduction of negative charge of the core AuNP surface by COOH-PEG ligands. (e) In a low pH environment where H^+ is abundant, both PEG and NH_2 are positively charged, and together greatly offset the negative charge of the AuNPs. (f) In a high pH environment, where Na^+ is abundant, the PEG is positively charged due to Na^+ binding, and NH_2 remains charge neutral. (g) At low pH, there is also highly likely that hydrogen bonds form between NH_2 and PEG, which promotes assembly.

The net negative charge present in the gold core, as demonstrated in Fig. 10 (a) is likely due to chlorine ions that are left over from the AuNPs growth process[47,48] and is also inferred in an earlier X-ray reflectivity study.[49] After grafting with PEG, the negative charge of the core is offset by approximately 28 protons

that are hydrogen-bonded to the ether oxygen of PEG. The apparent positive charge of PEG, demonstrated in Fig. 10 (b), supports the idea that PEG acts like a polyelectrolyte by sequestration of cations.[50–52] The terminal carboxylic group adds about $10e$ to that of neutral PEG, at near neutral pH, as it is protonated, as is illustrated in Fig. 10 (c). Finally, for the PEG terminated with amine there are approximately $+33e$ added compared to the PEG with methyl terminal, as is illustrated in Fig. 10 (e).

The PEG chains and their COOH terminals act as H^+ acceptors and donors at near neutral pH and thus bind to each other, consistent with the view that the COOH-PEG corona partially collapses rendering the grafted particle a smaller effective hydrodynamic diameter compared to those of the CH$_3$- and NH$_2$-PEG capped PEG-AuNPs. At low pH, COOH stays charge-neutral while PEG becomes positively charged by acquiring protons or hydronium ions, thus offsets the negative charge of the AuNPs, and assembly of particles is favored. At high pH, i.e., high [NaOH], COOH is deprotonated and highly charged, and this additional negative charge offsets the PEG's positive charge associated with bound Na$^+$, thus the dispersion state of particles is favored.

On the other hand, NH$_2$ terminal, in and of itself, is a proton acceptor that enhances total number of positive protons to offset the negative surface charge of the AuNPs. At low pH where positive protons and hydronium ions are abundant, the positively charged NH$_2$ terminals, along with positive PEG, greatly offset the intrinsic residual negative charge of AuNPs (see Fig. 10 (d)). At high pH where NH$_2$ terminal remain charge-neutral, PEG still harvest Na$^+$ in an Na$^+$ rich environment and thus carry positive charge (see Fig. 10 (e)), thus still offset the negative charge of the AuNP significantly. Therefore, both PEG and NH$_2$ can together reduce the negative charge of AuNPs, and even inverse the charge polarity from negative to positive, which explains why NH$_2$-PEG-AuNPs favors assembly in a much wider pH range than COOH-PEG-AuNPs.

Thus, our theoretical considerations to rationalize the results in the framework of the
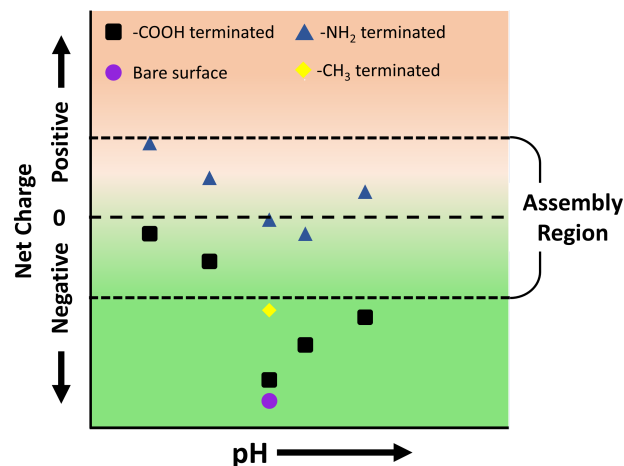
Figure 11: Conceptual illustration for the easiness of assembly of PEG-AuNPs regulated by pH. When the net charge of the PEG-AuNP near zero (i.e., charge neutral), they assemble, and disperse otherwise.

Poisson-Boltzmann theory explain the assembly behavior of both the COOH- and NH$_2$-PEG capped AuNPs. It is worth noting that NH$_2$ terminals also form hydrogen bonds with the ether oxygen in PEG at low pH when proton is abundant, as shown in Fig. 10 (g). This may be the main reason why charged NH$_2$ terminals also promote assembly regardless of pH. A more thorough molecular simulation study is underway to shed more light on this regard.

The PB based perspective also helps understand the assembly driven by K$_2$CO$_3$, when cations concentration, [K$^+$], is orders of magnitude higher than that of Na$^+$ at comparable pH levels (see Fig. 7). Even though COOH terminals are deprotonated and thus negatively charged, PEG may acquire enough K$^+$ to neutralize the whole particle to trigger assembly. Figure 11 provides a conceptual illustration of PB-theory based understanding. The NH$_2$-PEG harvest positive charge that greatly offset the intrinsic negative charge of the AuNPs when there is abundance of H$^+$ (i.e., low pH) and Na$^+$ (i.e., high pH) in the solution, resulting with a neutral NP prone to assembly. While COOH-PEG only offset AuNP negative surface charge with abundance of H$^+$ to assemble. At high pH, the deprotonated carboxylic group carry negative charge, partially cancels

out the PEG positive charge arising from the bound Na^+ ions.

Conclusions

NPs decorated with opposite surface charges can constitute building blocks of ionic colloidal crystals yielding another control knob to achieve super-stoichiometry. As we embark on assembling NPs of opposite charges, we start by studying the properties and assembly of PEG-AuNPs of like charge. Here, we report the results of ligand PEG with various terminal groups, i.e., CH_3 (neutral), NH_2 (positively charged), and COOH (negatively charged). Dynamic light scattering measurements show that the hydrodynamic diameter of NH_2-PEG-AuNP (core and PEG-corona) is slightly larger ($\sim 5\%$) than that of CH_3-PEG-AuNP, while COOH-PEG-AuNP is significantly smaller ($\sim 18\%$). The ζ potentials are associated with the expected charge for the terminal groups. The net charge of the grafted AuNPs affect their assembly at the vapor/liquid interface. Using surface sensitive synchrotron X-ray diffraction techniques, we find that the grafted AuNPs with NH_2 spontaneously migrate to the surface and form a two-dimensional hexagonal structure with similar lattice constant to one obtained with a neutral terminal group CH_3 in the presence K_2CO_3. The COOH-PEG-AuNPs migrate and form 2D hexagonal structure on the aqueous surface only at moderately high salt (100 mM K_2CO_3) concentrations, with significantly smaller lattice constant. The aqueous pH regulates the assembly and dispersion behavior of COOH-PEG-AuNPs but has nearly no effect on that of NH_2-PEG-AuNPs. The difference in the assembly behavior of COOH-PEG-AuNPs and NH_2-PEG-AuNPs in response to pH and salinity regulation is attributed to the intrinsic residual negative charge on AuNP's surface and PEG's sequestration of cations that make up a significant portion of the net charge, other than the charge of the ligand terminals upon protonation or deprotonation. The fact that NH_2-PEG-AuNPs readily assemble even at low pH suggests that the coupling interaction between NH_2 terminal group and PEG, most likely hydrogen bonding, may promote spontaneous assembly. Our results, dealing with charged AuNPs, pave the way to ongoing future work to assemble oppositely charged grafted NPs into binary superionic crystals analogous to atomistic ionic crystals.

Acknowledgements

References

1. Andres, R. P.; Bein, T.; Dorogi, M.; Feng, S.; Henderson, J. I.; Kubiak, C. P.; Mahoney, W.; Osifchin, R. G.; Reifenberger, R. Coulomb staircase at room temperature in a self-assembled molecular nanostructure. *science* **1996**, *272*, 1323–1325.

2. Chen, S.; Ingram, R. S.; Hostetler, M. J.; Pietron, J. J.; Murray, R. W.; Schaaff, T. G.; Khoury, J. T.; Alvarez, M. M.; Whetten, R. L. Gold nanoelectrodes of varied size: transition to molecule-like charging. *Science* **1998**, *280*, 2098–2101.

3. Perenboom, J. A. A. J.; Wyder, P.; Meier, F. Electronic properties of small metallic particles. *Physics Reports* **1981**, *78*, 173–292.

4. Link, S.; El-Sayed, M. A. Size and temperature dependence of the plasmon absorption of colloidal gold nanoparticles. *The Journal of Physical Chemistry B* **1999**, *103*, 4212–4217.

5. Lu, A.-H.; Salabas, E. e.; Schüth, F. Magnetic nanoparticles: synthesis, protection, functionalization, and application. *Angewandte Chemie International Edition* **2007**, *46*, 1222–1244.

6. Haase, M.; Schäfer, H. Upconverting nanoparticles. *Angewandte Chemie International Edition* **2011**, *50*, 5808–5829.

7. Zhan, C.; Chen, X.-J.; Yi, J.; Li, J.-F.; Wu, D.-Y.; Tian, Z.-Q. From plasmon-enhanced molecular spectroscopy to plasmon-mediated chemical reactions. *Nature Reviews Chemistry* **2018**, *2*, 216–230.

8. Daniel, M.-C.; Astruc, D. Gold nanoparticles: assembly, supramolecular chemistry, quantum-size-related properties, and applications toward biology, catalysis, and nanotechnology. *Chemical reviews* **2004**, *104*, 293–346.

9. Fan, J. A.; Wu, C.; Bao, K.; Bao, J.; Bardhan, R.; Halas, N. J.; Manoharan, V. N.; Nordlander, P.; Shvets, G.; Capasso, F. Self-assembled plasmonic nanoparticle clusters. *science* **2010**, *328*, 1135–1138.

10. Talapin, D. V.; Lee, J.-S.; Kovalenko, M. V.; Shevchenko, E. V. Prospects of colloidal nanocrystals for electronic and optoelectronic applications. *Chemical reviews* **2010**, *110*, 389–458.

11. Ghosh, S. K.; Pal, T. Interparticle Coupling Effect on the Surface Plasmon Resonance of Gold Nanoparticles: From Theory to Applications. *Chem. Rev.* **2007**, *107*, 4797–4862.

12. Bishop, K. J. M.; Wilmer, C. E.; Soh, S.; Grzybowski, B. A. Nanosclae Forces and Their Uses in Self-assembly. *Small* **2009**, *5*, 1600–1630.

13. Si, K. J.; Chen, Y.; Shi, Q.; Cheng, W. Nanoparticle Superlattices: The Roles of Soft Ligands. *Adv. Sci.* **2018**, *5*, 1700179.

14. Grzelczak, M.; Liz-Marzán, L. M.; Klajn, R. Stimuli-responsive self-assembly of nanoparticles. *Chemical Society Reviews* **2019**, *48*, 1342–1361.

15. Nykypanchuk, D.; Maye, M. M.; Van Der Lelie, D.; Gang, O. DNA-guided crystallization of colloidal nanoparticles. *Nature* **2008**, *451*, 549–552.

16. Park, S. Y.; Lytton-Jean, A. K.; Lee, B.; Weigand, S.; Schatz, G. C.; Mirkin, C. A. *Spherical Nucleic Acids*; Jenny Stanford Publishing, 2020; pp 515–525.

17. Laramy, C. R.; O'Brien, M. N.; Mirkin, C. A. *Spherical Nucleic Acids*; Jenny Stanford Publishing, 2020; pp 227–289.

18. Macfarlane, R. J.; Lee, B.; Jones, M. R.; Harris, N.; Schatz, G. C.; Mirkin, C. A. *Spherical Nucleic Acids*; Jenny Stanford Publishing, 2020; pp 539–553.

19. Zhang, H.; Wang, W.; Mallapragada, S.; Travesset, A.; Vaknin, D. Macroscopic and Tunable Nanoparticle Superlattices. *Nanoscale* **2017**, *9*, 164–171.

20. Zhang, H.; Wang, W.; Mallapragada, S.; Travesset, A.; Vaknin, D. Ion-specific interfacial crystallization of polymer-grafted nanoparticles. *The Journal of Physical Chemistry C* **2017**, *121*, 15424–15429.

21. Zhang, H.; Wang, W.; Akinc, M.; Mallapragada, S.; Travesset, A.; Vaknin, D. Assembling and ordering polymer-grafted nanoparticles in three dimensions. *Nanoscale* **2017**, *9*, 8710–8715.

22. Zhang, H.; Nayak, S.; Wang, W.; Mallapragada, S.; Vaknin, D. Interfacial self-assembly of polyelectrolyte-capped gold nanoparticles. *Langmuir* **2017**, *33*, 12227–12234.

23. Kim, H. J.; Wang, W.; Bu, W.; Hossen, M. M.; Londono-Calderon, A.; Hillier, A. C.; Prozorov, T.; Mallapragada, S.; Vaknin, D. Salt mediated self-assembly of poly (ethylene glycol)-functionalized gold nanorods. *Scientific reports* **2019**, *9*, 1–9.

24. Kim, H. J.; Wang, W.; Travesset, A.; Mallapragada, S. K.; Vaknin, D. Temperature-induced tunable assembly of columnar phases of nanorods. *ACS nano* **2020**, *14*, 6007–6012.

25. Kim, H. J.; Hossen, M. M.; Hillier, A. C.; Vaknin, D.; Mallapragada, S. K.; Wang, W. Interfacial and bulk assembly of anisotropic gold nanostructures: implications for photonics and plasmonics. *ACS Applied Nano Materials* **2020**, *3*, 8216–8223.

26. Minier, S.; Kim, H. J.; Zaugg, J.; Mallapragada, S. K.; Vaknin, D.; Wang, W. Poly (N-isopropylacrylamide)-grafted gold nanoparticles at the vapor/water interface. *Journal of Colloid and Interface Science* **2021**, *585*, 312–319.

27. Kim, H. J.; Wang, W.; Mallapragada, S.; Travesset, A.; Vaknin, D. Nanoparticle Superlattices with Negative Thermal Expansion (NTE) Coefficients. *The Journal of Physical Chemistry C* **2021**, *125*, 10090–10095.

28. Kim, H. J.; Wang, W.; Mallapragada, S. K.; Vaknin, D. The Effects of Temperature on the Assembly of Gold Nanoparticle by Interpolymer Complexation. *The Journal of Physical Chemistry Letters* **2021**, *12*, 1461–1467.

29. Kim, H. J.; Wang, W.; Zhang, H.; Freychet, G.; Ocko, B. M.; Travesset, A.; Mallapragada, S. K.; Vaknin, D. Effect of polymer chain length on the superlattice assembly of functionalized gold nanoparticles. *Langmuir* **2021**, *37*, 10143–10149.

30. Kim, H. J.; Wang, W.; Zhang, H.; Freychet, G.; Ocko, B. M.; Travesset, A.; Mallapragada, S. K.; Vaknin, D. Binary superlattices of gold nanoparticles in two dimensions. *The Journal of Physical Chemistry Letters* **2022**, *13*, 3424–3430.

31. Wang, W.; Zhang, H.; Mallapragada, S.; Travesset, A.; Vaknin, D. Ionic depletion at the crystalline Gibbs layer of PEG-capped gold nanoparticle brushes at aqueous surfaces. *Physical Rview Materials* **2017**, *1*, 076002.

32. Kalsin, A. M.; Kowalczyk, B.; Smoukov, S. K.; Klajn, R.; Grzybowski, B. A. Ionic-like Behavior of Oppositely Charged Nanoparticles. *J. Am. Chem. Soc.* **2006**, *128*, 15046–15047.

33. Kastilani, R.; Wong, R.; D., P. L. Efficient Electrosteric Assembly of Nanoparticle Heterodimers and Linear Heteroassemblies. *Langmuir* **2018**, *34*, 826–836.

34. Bridonneau, N.; Voël, V.; Zrig, S.; Carn, F. Self-Assembly of Gold Nanoparticles with Oppositely Charged, Long, Linear Chains of Periodic Copolymers. *J. Phys. Chem. B* **2020**, *124*, 900–908.

35. Curk, T.; E., L. Charge Regulation Effects in Nanoparticle Self-Assembly. *Phys. Rev. Lett.* **2021**, *126*, 138003.

36. Pothukuchi, R. P.; Prajapat, V. K.; Radhakrishna, M. Charge-Driven Self-Assembly of Polyelectrolyte-Grafted Nanoparticles in Solutions. *Langmuir* **2021**, *37*, 12007–12015.

37. Grier, D. G. A surprisingly attractive couple. *Nature* **1998**, *393*, 621.

38. Bowen, W. R.; Sharif, A. O. Long-range electrostatic attractionbetweenlike-charge spheres in a charged pore. *Nature* **1998**, 663–665.

39. Wu, L.; Wang, X.; Wang, G.; Chen, G. In situ X-ray scattering observation of two-dimensional interfacial colloidal crystallization. *Nature Communications* **2018**, *9*, 1335.

40. dos Santos, A. P.; Levin, Y. Like-charge Attraction between Metal Nanoparticles in a 1:1 Electrolyte Solution. *Phys. Rev. Lett.* **2019**, *122*, 248005.

41. Rosenberg, M.; Dekker, F.; Donaldson, J. G.; Philipse, A. P.; Kantorovich, S. S. Self-assembly of charged colloidal cubes. *Soft Matter* **2020**, *16*, 4451–4461.

42. Benoit, D. N.; Zhu, H.; Lilierose, M. H.; Verm, R. A.; Ali, N.; Morrison, A. N.; Fortner, J. D.; Avendano, C.; Colvin, V. L. Measuring the Grafting Density of Nanoparticles in Solution by Analytical Ultracentrifugation and Total Organic Carbon Analysis. *Analytical Chemistry* **2012**, *84*, 9238–9245, PMID: 22967239.

43. Als-Nielsen, J.; Desmond, M. *Elements of Modern X-ray Physics*, 2nd ed.; Wiley, 2011.

44. Nayak, S.; Fieg, M.; Wang, W.; Bu, W.; Mallapragada, S.; Vaknin, D. Effect of (Poly)electrolytes on the Interfacial Assembly of Poly(ethylene glycol)-Functionalized Gold Nanoparticles. *Langmuir* **2019**, *35*, 2251–2260.

45. Londoño-Calderon, A.; Wang, W.; Lawrence, J. J.; Bu, W.; Vaknin, D.; Prozorov, T. Salt-Induced Liquid–Liquid Phase Separation and Interfacial Crystal Formation in Poly (N-isopropylacrylamide)-Capped Gold Nanoparticles. *The Journal of Physical Chemistry C* **2021**, *125*, 5349–5362.

46. Avazbaeva, Z.; Sung, W.; Lee, J.; Phan, M. D.; Shin, K.; Vaknin, D.; Kim, D. Origin of the instability of octadecylamine Langmuir monolayer at low pH. *Langmuir* **2015**, *31*, 13753–13758.

47. Doane, T. L.; Cheng, Y.; Babar, A.; Hill, R. J.; Burda, C. Electrophoretic Mobilities of PEGylated Gold NPs. *Journal of the American Chemical Society* **2010**, *132*, 15624–15631.

48. Doane, T. L.; Chuang, C.-H.; Hill, R. J.; Burda, C. Nanoparticle ζ-potentials. *Accounts of chemical research* **2012**, *45*, 317–326.

49. Wang, W.; Zhang, H.; Kuzmenko, I.; Mallapragada, S.; Vaknin, D. Assembling bare Au nanoparticles at positively charged templates. *Scientific reports* **2016**, *6*, 1–9.

50. Cao, N.; Zhao, Y.; Chen, H.; Huang, J.; Yu, M.; Bao, Y.; Wang, D.; Cui, S. Poly (ethylene glycol) Becomes a Supra-Polyelectrolyte by Capturing Hydronium Ions in Water. *Macromolecules* **2022**, *55*, 4656–4664.

51. Fang, Y.; Giesecke, M.; Furo, I. Complexing cations by poly (ethylene oxide): Binding site and binding mode. *The Journal of Physical Chemistry B* **2017**, *121*, 2179–2188.

52. Hakem, I. F.; Lal, J.; Bockstaller, M. R. Binding of monovalent ions to PEO in solution: Relevant parameters and structural transitions. *Macromolecules* **2004**, *37*, 8431–8440.

Two-dimensional assembly of nanoparticles grafted with charged-end-group polymers

Hyeong Jin Kim,[†] Binay P. Nayak,[†] Honghu Zhang,[‡] Benjamin M. Ocko,[¶] David Vaknin,[§] Alex Travesset,[§] Surya K. Mallapragada,[*,†] and Wenjie Wang[*,||]

[†]*Ames National Laboratory, and Department of Chemical and Biological Engineering, Iowa State University, Ames, Iowa 50011, United States*
[‡]*NSLS-II, Brookhaven National Laboratory, Upton, New York 11973, United States*
[¶]*Center for Functional Nanomaterials and NSLS-II, Brookhaven National Laboratory, Upton, New York 11973, United States*
[§]*Ames National Laboratory, and Department of Physics and Astronomy, Iowa State University, Ames, Iowa 50011, United States*
[||]*Division of Materials Sciences and Engineering, Ames National Laboratory, U.S. DOE, Ames, Iowa 50011, United States*

E-mail: suryakm@iastate.edu; wenjiew@ameslab.gov

Simple calculation of the pH for K_2CO_3 solutions

The K_2CO_3 stock solution was prepared with nominal amount of K_2CO_3 dissolved in pure water and further dilute to the nanoparticle suspensions to specified concentration. The pH is determined in terms of known equilibrium constants for room temperature via textbook style calculation, rather than actual measurements. The CO_3^{2-} is the conjugate base of the weak acid HCO_3^- with its known acid dissociation constant, $K_a = 4.7 \times 10^{-11}$, for $K_a = [CO_3^{2-}][H^+]/[HCO_3^-]$. So for the equilibrium $CO_3^{2-} + H_2O \rightleftharpoons HCO_3^- + OH^-$, the corresponding base dissociation constant $K_b = K_w/K_a = 2.12 \times 10^{-4}$, where K_w is the dissociation constant of water $(=10^{-14})$. Thus, we determine $[OH^-]$ based on the known $[K_2CO_3]$, assuming $[OH^-] \approx [HCO_3^-]$ and $[HCO_3^-] \ll [CO_3^{2-}]$ in the aqueous solution. So the pH equals to $14 + \log_{10}(\sqrt{K_b \times [K_2CO_3]})$. For $[K_2CO_3] = 1$, 10, 100 mM, the corresponding pH=10.7, 11.2, 11,7, respectively.

Grafting density from TGA

To calculate the grafting density from TGA using Eq. S1, first, the relative mass of the PEG shell and gold nanoparticles was calculated from Fig. S1. The total number of polymer chains was calculated by dividing the weight of the PEG from the experiment by the mass of each chain of PEG which is 5 kDa or 8.2027×10^{-21} gm. The total number of nanoparticles was calculated by dividing the weight of the nanoparticles from the experiment with the mass of individual nanoparticles calculated by multiplying the volume of each nanoparticle, assuming it is to be in the spherical shape of diameter 9.34 nm (calculated from form factor) and having a density of 19.6 g/cm^3. Since we are calculating the grafting density as chains per nm^2, we need to divide the total area of nanoparticles, which is calculated again, assuming it to be the spherical shape of diameter 9.34 nm.

$$\sigma_{TGA} = \frac{\rho_{NP}}{6} \times \frac{PEG \ wt\%}{NP \ wt\%} \times \frac{D_{NP}}{MW_{PEG}}. \tag{S1}$$
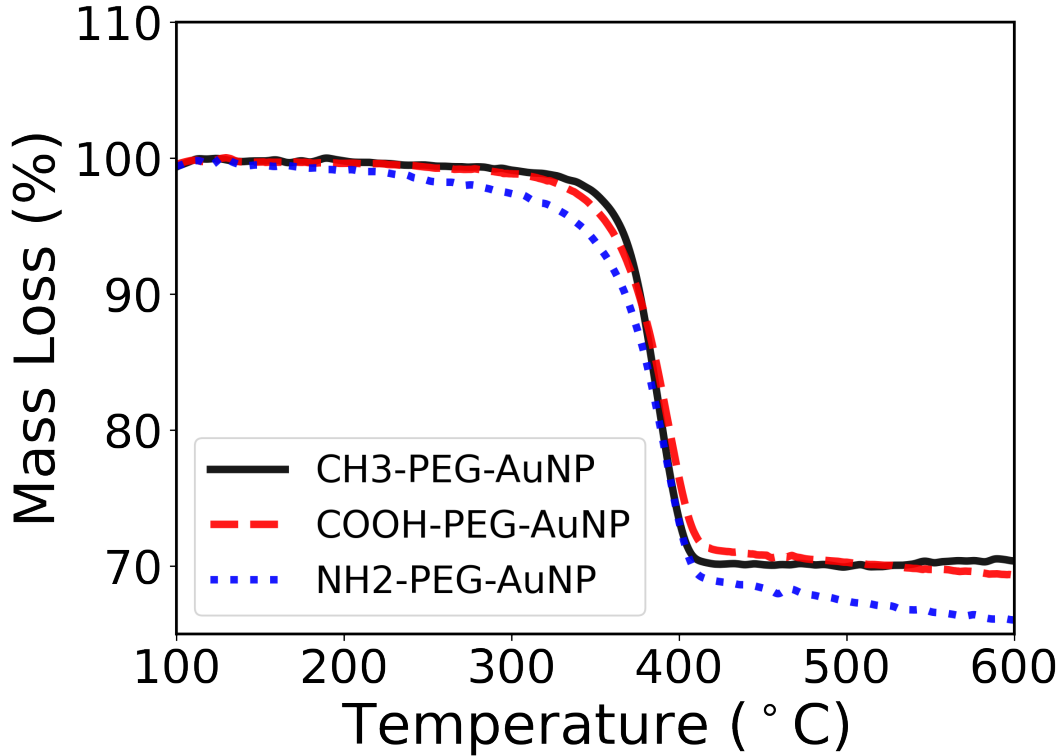
Figure S1: TGA showing relative mass loss percentage as a function of the temperature of polymer grafted AuNPs.

where σ_{TGA} is the grafting density, wt% is the calculated change in relative weight, ρ_{NP} is the mass density of gold, and $\mathrm{MW}_{\mathrm{PEG}}$ represents the molecular weight of PEG.

Electrostatic Calculation: Poisson Boltzmann equation

Using the Poisson-Boltzmann formalism and the known pKa values for the terminal groups we calculate surface charges and ζ-potential for the two charged terminal groups. The electric potential $\psi(r)$ is related to electric field as follows,

$$E(r) = -\frac{d\psi(r)}{dr} \ . \tag{S2}$$

There are $a = 1 \cdots f$ ion species (with charge eq_a), with number density given by Boltzmann statistics

$$n_a(r) = \frac{1}{\upsilon} e^{\frac{\mu_a}{k_B T}} e^{-q_a \frac{e\psi(r)}{k_B T}} \ , \tag{S3}$$

where υ is a reference volume and μ_a the corresponding chemical potential. The Poisson-Boltzmann equation is

$$\frac{1}{r^2} \frac{d}{dr} \left(r^2 \frac{d\psi(r)}{dr} \right) = -\frac{e}{\varepsilon_0 \varepsilon_w} \sum_{a=1}^{f} q_a n_a(r)$$

$$= -\frac{e}{\varepsilon_0 \varepsilon_w} \sum_{a=1}^{f} q_a n_a^{\infty} e^{-q_a e \frac{\psi(r)}{k_B T}} \ . \tag{S4}$$

The above equation is

$$\frac{1}{r^2}\frac{d}{dr}\left(r^2 E(r)\right) = \frac{e}{\varepsilon_0 \varepsilon_w} \sum_{a=1}^{f} q_a n_a^\infty e^{-q_a e \frac{\psi(r)}{k_B T}}.$$

(S5)

which implies, with R the NP radius with a wall located at a distance L

$$L^2 E(L) - r^2 E(r)$$

$$= \frac{e}{\varepsilon_0 \varepsilon_w} \int_r^L r^2 dr \sum_{a=1}^{f} q_a n_a^\infty e^{-q_a e \frac{\psi(r)}{k_B T}}.$$

(S6)

It is $E(L) = 0$, hence

$$-R^2 E(R) = \frac{e}{\varepsilon_0 \varepsilon_w} \int_L^R r^2 dr \sum_{a=1}^{f} q_a n_a^\infty e^{-q_a e \frac{\psi(r)}{k_B T}}$$

$$= -\frac{\sigma}{\varepsilon_0 \varepsilon_w} R^2 \to E(R) = \frac{\sigma}{\varepsilon_0 \varepsilon_w}.$$

In dimensionless variables $u = r/\lambda_{DB}$, $\phi = \frac{e\psi}{k_B T}$ where $\lambda_{DB}^2 = 1/(8\pi l_B I)$, with l_B the Bjerrum length and I the ionic strength. The PB equation is

$$\frac{1}{u^2}\frac{d}{du}\left(u^2 \frac{d\phi(u)}{du}\right) = -\sum_{a=1}^{\infty} \frac{q_a n_a^\infty}{2I} e^{-q_a \phi(u)},$$

(S7)

with boundary condition

$$\frac{d\phi}{du} = -2 \,\mathrm{sign}(\sigma)\frac{\lambda_{DB}}{\lambda_{GC}}.$$

(S8)

where $\lambda_{GC} = \frac{e}{2\pi l_B \sigma}$ is the Guoy-Champan length. Within the linear approximation

$$\frac{1}{u^2}\frac{d}{du}\left(u^2 \frac{d\phi(u)}{du}\right) = \phi(u).$$

(S9)

The solution for the potential and electric field is

$$\phi(u) = 2 \,\mathrm{sign}(\sigma)\frac{\hat{R}^2}{\hat{\lambda}_{GC}} \frac{1 - \frac{\hat{L}+1}{\hat{L}-1}e^{-2(\hat{L}-u)}}{1 - \frac{(\hat{R}-1)(\hat{L}+1)}{(\hat{R}+1)(\hat{L}-1)}e^{-2(\hat{L}-\hat{R})}} \frac{e^{-(u-\hat{R})}}{u(1+\hat{R})}$$

(S10)

$$E(u) = 2 \,\mathrm{sign}(\sigma)\frac{\hat{R}^2}{\hat{\lambda}_{GC}} \frac{u+1-(u-1)\frac{\hat{L}+1}{\hat{L}-1}e^{-2(\hat{L}-u)}}{1 - \frac{(\hat{R}-1)(\hat{L}+1)}{(\hat{R}+1)(\hat{L}-1)}e^{-2(\hat{L}-\hat{R})}} \frac{e^{-(u-\hat{R})}}{u^2(1+\hat{R})}$$

$\hat{R} = \frac{R}{\lambda_{DB}}$, $\hat{L} = \frac{L}{\lambda_{DB}}$ and $\hat{\lambda}_{GC} = \frac{\lambda_{GC}}{\lambda_{DB}}$.

Comparing the linear solution to the exact one from Eq. S7 the difference for the situations considered here is within 5% at worst (at zero salt concentration, pH=7). Hence, there is negligible error in using the linear solution and keeping the ion distribution as in Eq. S3, that is, without Taylor-expanding the exponential.